Density Functional Characterization of the Chemoselective Oxidation of Catechol by using Molecular Oxygen: Thermodynamics of the Reaction between [(triphos)Ir(dtbc)]$^+$ and O_2

Alessandro Bencini,*[a] Eckhard Bill,[b] Andrea Scozzafava,[a] and Federico Totti[a]

Abstract: The catalytic mechanism of *intra* and *extra* catechol cleaving dioxygenases is still a matter of debate, because the intermediate transient oxygen adduct has never been isolated in these enzymes. The complex [(triphos)Ir(dtbc)]$^+$ (triphos = $MeC(CH_2PPh_2)_3$, $DBTC^{2-}$ = 3,5-di-*tert*-butylcatecholate), reacts with molecular oxygen and exhibits a ring-cleaving catalytic activity, and a stable oxygen intermediate appears; this stimulates an opportunity for obtaining information that can be transferable to the above-mentioned enzymatic catalytic centers, therefore, giving a breakthrough into the strategy of oxygen activation in these natural systems. Here, we present the results of our computational approach, based on density functional theory, focusing on the following aspects: to explain the interaction with molecular oxygen and how to avoid the existing spin problem, to understand the formation of the bridging moiety, to clarify, if any, the possible influence on the structure of the formed adduct of the bidentate versus monodentate binding of the catechol ligand, and to disclose, eventually, the nature of final decomposition products with the aim to rationalize the *intra* versus *extra* cleavage of the catechol molecule itself.

Keywords: catechol · density functional calculations · iridium · reaction mechanisms · reactivity

Introduction

When coordinated to a metal center, catechol and some of its derivatives[1] can react with molecular oxygen (dioxygen) undergoing ring-cleavage reactions that lead to aliphatic (muconic) derivatives. This reaction is of particular significance in nature, because it leads to the degradation pathway of aromatic substances spread in the biosphere[2] by microorganisms that use them as a carbon source, hence, allowing them to get all their carbon and energy from aromatic sources.[3] This class of reactions therefore represents a key step in the whole bio-geochemical carbon cycle.

In microorganisms, this reaction is enzyme-assisted by the so called *ring-opening dioxygenases*, which are metalloenzymes that usually contain non-heme iron in their active sites. These dioxygenases can selectively open the catechol ring in two different ways as shown in Scheme 1.

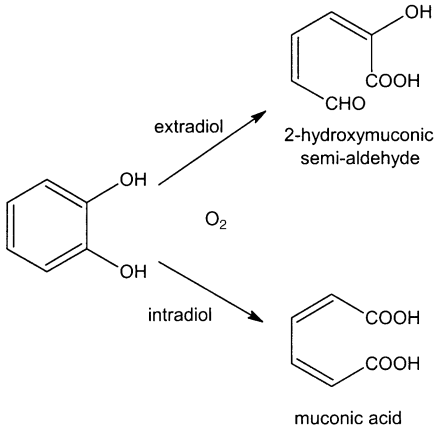

Scheme 1. The two ways in which dioxegenases can selectively open the catechol ring.

The *intradiol dioxygenases* catalyze the cleavage of the carbon–carbon bond between the two hydroxyl groups and contain Fe^{III} in their active site; the *extradiol dioxygenases* catalyze the cleavage of the carbon–carbon bond adjacent to one of the oxygens and contain Fe^{II}.[4] Six crystal structures of the naturally occurring enzymes have been determined so far,[5, 6] showing that in the intradiol dioxygenases[5] the Fe^{III} ion is coordinated by two histidines, two tyrosines, and one water molecule, and that in the extradiol dioxygenases[6] the Fe^{II} ion is coordinated by two hystidines, one glutamic acid,

[a] Prof. A. Bencini, Prof. A. Scozzafava, Dr. F. Totti
Dipartimento di Chimica, Polo Scientifico
Università degli Studi di Firenze
Via della Lastruccia, 3
50019 Sesto F.no (Italy)
Fax: (+39) 055-457-3372
E-mail: alessandro.bencini@unifi.it

[b] Prof. E. Bill
Max-Planck-Institut für Strahlenchemie
Mülheim (Germany)

 DOI: 10.1002/chem.200304710

and two water molecules. A large number of spectroscopic and kinetic investigations[4, 7] have been performed on both classes of enzymes in order to get an insight into the intra- and extradiol cleavage mechanisms, and to resolve the riddle of the high specificity of each class of enzyme, that leads to the formation of specific intra- or extradiol cleavage products. Structural information on the adducts between the substrate and the enzymes became recently available,[8] and indicated that a monoanionic catecholate binds the iron atom in the extradiol dioxygenases. The early hypothesis that the catecholate dianion binds the iron atom in the intradiol dioxygenases is still a controversy. No definitive structural information is available yet on intermediate ternary enzyme—substrate–oxygen adducts.[9, 7]

Two different reaction mechanisms have been proposed for the intra- and extradiol dioxygenases due to the different chemical properties of iron(II) and iron(III).[10] In particular, the extradiol ring cleavage was claimed to occur by the attack of O_2 on iron(II) followed by the formation of a distal hydroperoxide intermediate, whereas, for the intradiol ring cleavage reactions, the attack of O_2 on one carbon atom of the substrate, followed by the formation of a proximal hydroperoxide intermediate, was suggested. A common feature of all the above class of reactions that was not fully investigated is the spin-forbidden nature of the reaction. Indeed the reactions seem to occur with dioxygen in its ground triplet state, so, when added to the spin of the iron center, it causes the total spin to change. To overcome this problem a spin-pairing model was invoked,[11] and in recent density functional theory (DFT) calculations on simple model complexes, Funabiki and Yamazaki[12] used a spin quartet ground state for all the Fe^{III}/O_2 moieties without much justification. In the last case the overall spin was preserved if the final Fe^{III} complex was formed in the intermediate spin state $S = 3/2$. Oxygen uptake from Fe^{III}(tpa) complexes (TPA = tris(2-pyridylmethyl)amine) was recently found to occur by the formation of the Fe^{IV}–oxo intermediate through DFT calculations.[13]

During the past few years a number of iron–catecholate complexes[7, 10, 14] were synthesized and found to react with dioxygen, opening the aromatic ring; these reactions were therefore studied as models in vitro of the dioxygenases. These model studies gave much information on the possible dependence of the intra- and extraring opening reactions on different factors, such as the oxidation state of the metal, the nature of the ligands, either the catechols or the terminal ligands, the geometry of coordination, the nature of the environment, and so on.[7, 10, 14] Besides, a lot of information was gained on the structures and properties of reactants and products, but no oxygen adduct was isolated or characterized as a reaction intermediate.

Recently all the structural and kinetic data available in the literature for the intra- and extradiol dioxygenases, as well as for the inorganic complexes that mimicked their activity, have been re-examined by Bugg et al.[10mnot] in order to obtain an unified view of the reaction mechanism(s). They suggest that, although different initial reaction steps can be formulated for the two classes of reactions, including the possible different manner of coordination of catechol itself in the two types of enzymes, the extra- and the intradiol reaction pathways should converge to the same proximal peroxide intermediate. After the formation of this common intermediate, the reactions appear to be controlled by substrate stereochemical factors and by the coordination geometry of the iron center. In particular, they showed that even if Fe^{II}–catecholate complexes preferentially lead to extradiolic oxidations, the $TACN/FeCl_2$ complex[10mt] gave both intra- and extra-diolic oxidation products depending on the reaction conditions, such as, the type of substrate (di- or mono-anionic catecholates) and the presence of pyridine. In contrast, the $TACN/FeCl_3$ complex was found to preferentially give extradiol cleavage, under all the above-mentioned conditions. It is interesting to note that the Fe^{III}-containing dioxygenases, selectively form intradiol oxidation products, except in a few cases when smaller extradiol oxidation products were recovered.[15]

A number of model complexes containing metal ions different from iron have been also synthesized, in some cases by using metal ions isoelectronic to iron(II) or iron(III).[9] In particular, Bianchini et al.[10] showed in 1992, that the $[(triphos)Rh^{III}(dtbc)]^+$ and $[(triphos)Ir^{III}(dtbc)]^+$ cations (triphos = $MeC(CH_2PPh_2)_3$, $DTBC^{2-}$ = 3,5-di-*tert*-butylcatecholate), in the presence of dioxygen, catalyze both intra- and extradiol cleavage of the aromatic ring. For the complex $[(triphos)Ir(phencat)]^+$ (triphos = $MeC(CH_2PPh_2)_3$, phencat = phenantrene catecholate), which also reacts with molecular oxygen, a stable oxygen adduct was obtained and its X-ray structure was solved.[10u] In this adduct the oxygen molecule bridges iridium(III) and one of the carbon atoms of catechol, as shown in Figure 1.

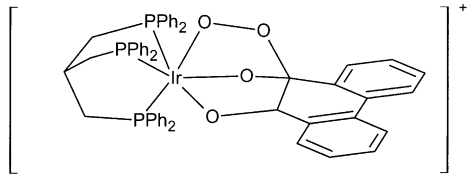

Figure 1. The structure of $[(triphos)Ir(phencat)]^+$.

The catechol was found to be distorted from planarity, acquiring a semiquinonate character. This oxygen adduct, in a complex that has ring-opening catalytic activity, is likely to represent the putative oxygen intermediate of the other inorganic models so far synthesized, and, possibly, the common intermediate of the intra- and extradiol dioxygenases suggested by Funabiki et al.[12] and Bugg et al.[10t]

It is apparent that only theoretical studies can improve the understanding of the reaction mechanism of the oxygen uptake reaction from the catecholates. Therefore, we decided to study this reaction in the simplest possible case, that is, the previously mentioned Ir(III) complex. The electronic structure of this complex is the simplest one, the available spin states being only singlet and triplet, and the only complex for which a stable intermediate dioxygen adduct was isolated. Previously, [16] we tested DFT against the known structures and spectroscopic properties of complexes with the general formula $[(triphos)M^{III}(CT)]^+$ (CT = catecholate) with M = Co and Ir, and we were also able to successfully reproduce

the structural features of the peroxy intermediate formed by the Ir complex. We also found that Co^{III} possesses a stable intermediate of similar structure.

In the present paper, we extend our previous study by applying DFT to characterize further steps of the reaction. In particular we want to examine how the binding mode of catecholate (i.e., monodentate/asymmetric vs bidentate/symmetric) influences the structure of the intermediate, the thermodynamics of several steps of the catalytic processes,[17] and how the formation of stable muconic acid and muconic semialdehyde derivatives can differentiate intra- and extradiol cleavage. Since the reaction is spin forbidden, we have computed its early stages on the lowest spin states of the system.

Rationalizing the reactivity of this inorganic complex towards oxygen and the evolution of the intermediate oxygen adduct should also help us to understand more clearly the reactivity and specificity of the active sites of the naturally occurring intra- and extradiol ring opening enzymes.

Computational details: All the calculations were performed by using DFT on the model systems $[(triphosH)Ir(CT)O_2]^+$ (CT^{2-} = catecholate dianion) and $[(triphosH)Ir(CTH)O_2]^{2+}$ (CTH^- = catecholate monoanion). In this system the real triphos ligand (triphos = $MeC(CH_2PPh_2)_3$) was modeled by replacing phenyl and methyl groups by hydrogen atoms (triphosH model ligand). The simplest catecholate dianion or monohydrogenated anion (CTH^-) were used as substrates instead of $phencat^{2-}$ or $DTBC^{2-}$. A schematic view of the model system $[(triphosH)Ir(CT)O_2]^+$ indicating the reference axes and the numbering of the atoms is shown in Figure 2. The same features also apply to $[(triphosH)Ir(CTH)O_2]^{2+}$ in which an H atom is bound to O4.

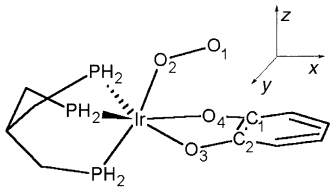

Figure 2. A schematic view of the model system $[(triphosH)Ir(CT)O_2]^+$.

The highest symmetry of the systems was in any case C_1. All the calculations were performed with the Gaussian98 program package, using the hybrid B3LYP functional.[18] The LANL2DZ relativistic effective core potentials and basis set for the metal and P atoms were used.[19] To C and H, the D95(d) basis was applied.[19]

Geometry optimizations were performed with internal coordinates, and frequencies were analytically computed in order to characterize the structures at the different stationary points.

Calculations were performed on the lowest lying singlet and triplet states of the oxygen adducts, $[(triphosH)Ir^{III}(CT)O_2]^+$ and $[(triphosH)Ir^{III}(CTH)O_2]^{2+}$, that arise from the possible occupations of the HOMO and LUMO orbitals (vide infra). A scan of the potential energy surfaces (PES) of the various spin states in the early stages of the reaction were performed by optimizing the geometry of the molecules in each spin state, and computing the energies of the other relevant spin states through single point calculations. Different starting geometries were used for geometry optimizations in order to look for the presence of local minima on the PES of the reactants. This procedure was applied to study the different coordination environments that could be relevant for concurring reaction pathways.

Results and Discussion

Geometric and electronic structure: Since dioxygen is paramagnetic (ground state $^3\Sigma_g^-$) and both the starting iridium(III) complexes and their adducts are diamagnetic (ground state ^1A), the reaction between the iridium complex and O_2 is an example of the so-called *spin-forbidden* reactions, that is, the spin multiplicity is not conserved during the event. This reaction, as well as a number of reactions with different substrates,[10u] were observed to occur even in the dark, ruling out the possibility that the effective reacting species is the O_2 molecule in its first excited singlet state ($^1\Delta_g$). Therefore, it seems plausible that, in the early stage, the reaction proceeds onto a triplet state PES until O_2 binds to the metal ion. The coordination of dioxygen to metal ions has been studied since 1963.[20] In a simplified molecular orbital scheme the degeneracy of the π* orbitals of O_2 is removed upon interaction with the 3d metal orbitals. This is shown in Figure 3 with an approximate orbital interaction diagram.

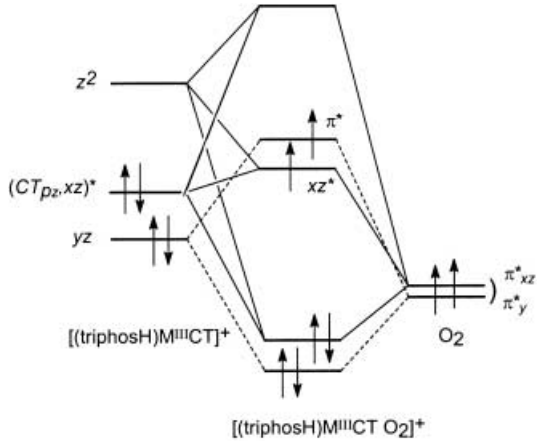

Figure 3. An approximate orbital interaction diagram.

The orbitals of the $[(triphosH)M^{(III)}(CT)]^+$ complex near the HOMO-LUMO region (on the left hand side in Figure 3) are mainly composed of the "axial" 3d orbitals of the metal center; these are antibonding with respect to the P and O atoms of the triphos, and the CT ligand.[16] The "in-plane" orbitals, $x^2 - y^2$ and xy, are σ antibonding and nonbonding and are not shown. The highest occupied molecular orbital (MOs) of dioxygen are labeled here as π_y^* and π_{xz}^* according to their orientation in the molecular frame (see Figure 2), the latter indicating the orbital which is perpendicular to the O–O direction and lies in the xz plane. The π_y^* orbital interacts with the yz-like orbital of the metal complex. This interaction

mainly occurs through a π-type overlap between the p_y orbital on O2 and the metal *yz* orbital. It is represented with dotted lines in Figure 3. The resulting MO is labeled as π*, since our calculations show it will mainly be localized on the π_y^* of dioxygen. The other relevant interaction of dioxygen occurs by a σ-type overlap between the π_{xz}^* and the HOMO – LUMO orbitals of the metal complex. From this interaction the orbital labeled as *xz** in Figure 3 results in the SOMO region. Although we label this here as orbital *xz**, its nature is more complex, and as a matter of fact, it contains a significant contribution from p_z orbitals of the catecholate anion; this is indicated as CTp_z in Figure 3. This simplified MO scheme shows that the singlet state arising from the double occupancy of the *xz** orbital, ^1A, can be stabilized with respect to the triplet state arising from the configuration ($xz^{*1}\pi^{*1}$). From this last configuration, one triplet and one singlet state (^3A, and $^1A(1)$) arise. We will call this last singlet state $^1A(1)$ to differentiate it from the ^1A state arising from the (xz^{*2}) configuration. Since all of these states have the same spatial symmetry and can have comparable energies, we included all of them in our calculations.[21] Transitions between triplet and singlet states are allowed by the spin-orbit coupling interaction, which can therefore account for the variation of the spin state of the system during the reaction.[22]

The structures of $[(triphosH)Ir^{III}(CT)(O_2)]^+$ (hereafter [**1**·O_2]) and $[(triphosH)Ir^{III}(CTH)(O_2)]^{2+}$ (hereafter [**2**·O_2]) optimized on the ^3A state are shown in Figure 4a and b respectively.

In order to find the most probable site of the attack of dioxygen, we started two geometry optimizations by placing dioxygen close to the metal center and to the catechol carbon atoms. At variance from the results previously reported for [**1**·O_2] in the ^1A state, dioxygen, even if initially located close to the carbon atoms of the catechol, binds to the metal atom in a η_1 mode in both the complexes. A similar attack was suggested to occur in small model systems containing iron.[12, 14] The overall symmetry of [**1**·O_2] is close to C_s, the symmetry plane being defined by O_2 and Ir. As a matter of fact, O_2 is bound to the iridium atom in such a way that the O2 atom is equidistant from the two carbon atoms of CT, while the O2 atom in [**2**·O_2] is closer to C(2). The Ir–O(1) distance in [**2**·O_2] is slightly longer than in [**1**·O_2] (2.127 Å vs 2.100 Å) and, consequently, the O(1)–O(2) distance shortens (1.340 in [**2**·O_2] vs 1.354 Å in [**1**·O_2]). By comparison with the O–O distance measured in the free dioxygen (1.208 Å),[23] an activation of the molecule is anticipated that does not vary significantly between [**1**·O_2] and [**2**·O_2]. The C(1)–C(2) bond length is also slightly different in the two systems (1.460 [**1**·O_2] vs 1.442 Å [**2**·O_2]) and significantly longer than that computed in the absence of O_2 (1.429 Å); this shows that the presence of dioxygen plays a significant role in the activation of the catechol ring. An iso-surface representation of the SOMOs computed for the [**1**·O_2] complex is shown in Figure 5.

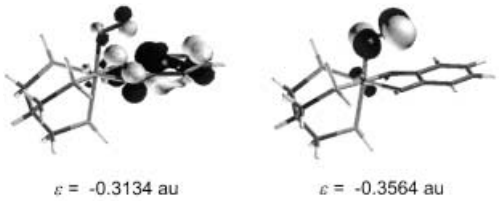

Figure 5. SOMOs of [**1**·O_2] in the ^3A state represented as isovalue surfaces ($\psi = \pm 0.05$ au). Their energies are also reported.

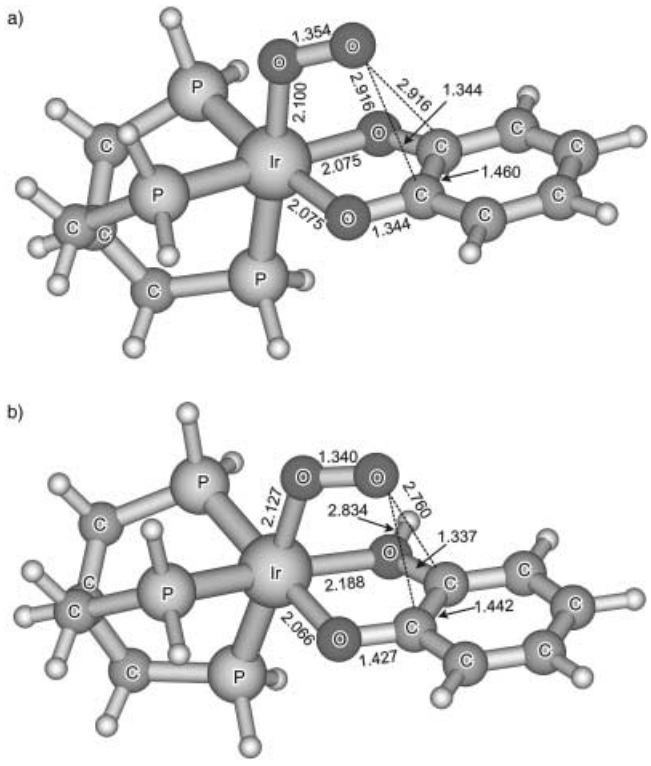

Figure 4. a) Optimized structure of [**1**·O_2] in the ^3A state; b) Optimized structure of [**2**·O_2] in the ^3A state. Relevant bond distances (Å) are shown.

These orbitals are mainly localized on the oxygen molecule and on the CT ligand, and represent the π_{xz}^* and *xz** orbitals of Figure 3, respectively. The Mulliken gross atomic population analysis assigns to the CT ligand the charge −0.071 e, which, relative to that computed in the absence of oxygen, −0.35 e, shows a significant increase. The computed charge on dioxygen is −0.31 e. With this in mind we can look at the complex as a $[(triphos)Ir^{III}(semiquinone)(superoxide)]^+$ species. Similar results were obtained for the [**2**·O_2] complex. The charge of the CTH ligand is now positive (0.44 e), due to the presence of the proton on one of the oxygen atoms. Also, C1 shows a lack of electron density with respect to C2 (0.34 e vs 0.40 e); as a result, C1 is expected to be the preferred site for a nucleophilic attack from the O2 atom. A small contribution from the 5d orbitals of the iridium atom is present in the SOMOs of both complexes. The charge on Ir is −0.44 e in the two cases.

The structures of $[(triphosH)Ir^{III}(CT)(O_2)]^+$ and $[(triphosH)Ir^{III}(CTH)(O_2)]^{2+}$ optimized on the $^1A(1)$ state are shown in Figure 6a and b, respectively.

Also in this case we used a different starting point for the geometry optimization in order to scan this singlet potential energy surface, and we obtained an energy minimum corresponding to geometries that are very close to the ones

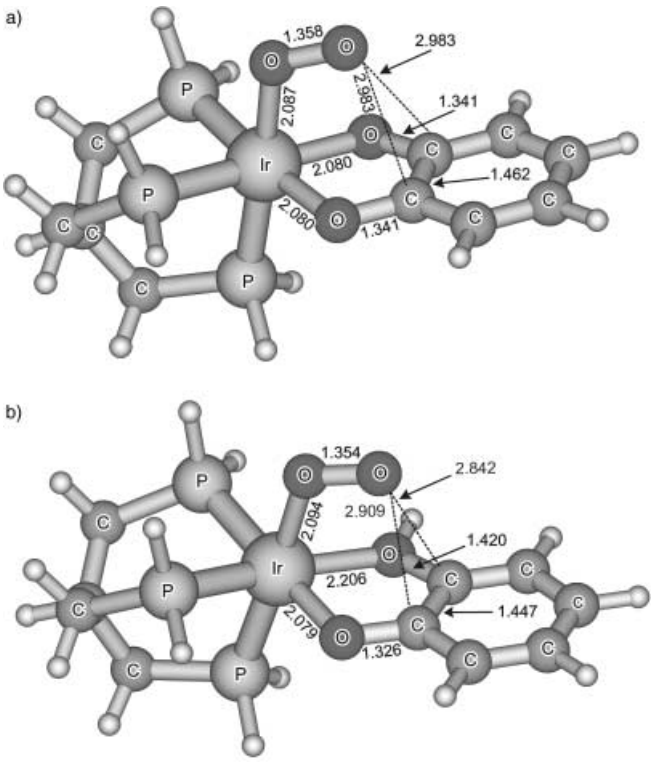

Figure 6. a) Optimized structure of $[\mathbf{1}\cdot O_2]$ in the ^{1}A(1) state; b) Optimized structure of $[\mathbf{2}\cdot O_2]$ in the ^{1}A(1) state. Relevant bond distances (Å) are shown.

obtained for the triplet state. The most relevant geometrical parameters of the optimized complexes are indicated in Figure 6a and b. The main differences with the geometries computed in the ^{3}A state are the lengthening of the O1–O2 distances (1.354 *vs* 1.358 and 1.340 vs 1.354 Å), the slight shortening of Ir–O1 (2.100 vs 2.087 and 2.127 vs 2.094 Å), and the increase of the O2–C1 and O2–C2 distances (2.916 vs 2.983 Å and 2.760/2.834 vs 2.842/2.909 Å). An iso-surface representation of the SOMOs computed for the $[\mathbf{1}\cdot O_2]$ complex is shown in Figure 7.

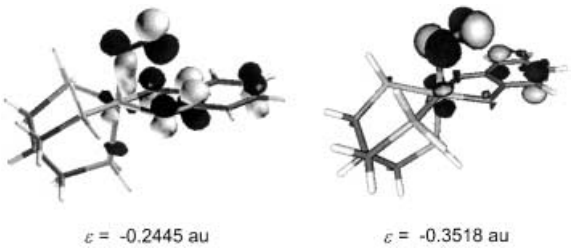

Figure 7. SOMOs of $[\mathbf{1}\cdot O_2]$ in the ^{1}A(1) state represented as isovalue surfaces ($\psi = \pm 0.05$ au). Their energies are also reported.

The SOMOs look similar to the ones shown in Figure 5 computed for the ^{3}A state. The Mulliken charges also do not change significantly from the ones computed on the ^{3}A state.

At variance with the previous results, the geometry optimizations of $[\mathbf{1}\cdot O_2]$ and $[\mathbf{2}\cdot O_2]$, performed on the ^{1}A state, gave structures close to the peroxy intermediate already characterized both experimentally and theoretically for $[\mathbf{1}\cdot O_2]$. The computed structures and the relevant geometrical parameters are shown in Figure 8a and b for $[\mathbf{1}\cdot O_2]$ and $[\mathbf{2}\cdot O_2]$, respectively.

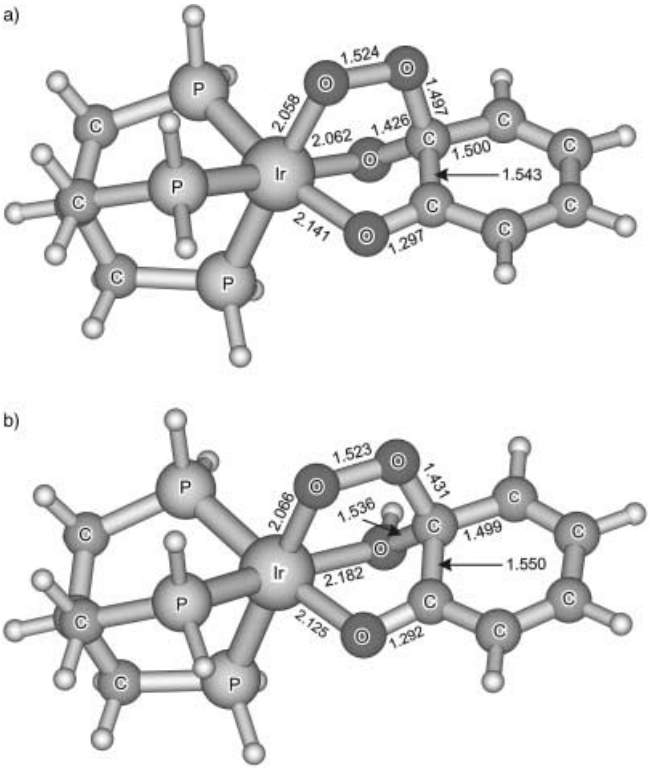

Figure 8. a) Optimized structure of the $[\mathbf{1}\cdot O_2]$ in the ^{1}A state; b) Optimized structure of the $[\mathbf{2}\cdot O_2]$ in the ^{1}A state. Relevant bond distances (Å) are shown.

In both complexes, the formation of the proximal peroxy intermediate breaks the aromaticity of the CT ring as shown by the marked sp^3 hybridization of C2. The bonds around the C2 atom are significantly lengthened, with respect to the deoxygenated substrates, by about 5–6% for $[\mathbf{1}\cdot O_2]$ and about 7–8% for $[\mathbf{2}\cdot O_2]$. It is worth mentioning that the geometries shown in Figure 8a and b can be obtained starting from the optimized structures of the ^{3}A and ^{1}A(1) states for $[\mathbf{1}\cdot O_2]$ and $[\mathbf{2}\cdot O_2]$. Geometry optimizations attempting to verify the stability of possible distal peroxy intermediates were performed for both systems; however, we get the proximal peroxy structure as a minumum.

It is interesting to note that for both systems $[\mathbf{1}\cdot O_2]$ and $[\mathbf{2}\cdot O_2]$, an initial attack of O_2 in its triplet ground state to the iridium center is found. This initial step is a spin allowed reaction that produces a well-defined metal–η^1-oxygen moiety. The enthalpy of this process is 41.7 and 19.1 kcal mol^{-1} for $[\mathbf{1}\cdot O_2]$ and $[\mathbf{2}\cdot O_2]$, respectively. This step is also the most exothermic one of the whole reaction. Since the iridium–peroxy–catecholate adduct is a diamagnetic species, in agreement with the experimental findings,[10u] the ground state of the system must change from triplet to singlet state to allow the reaction to proceed; this can be reasonably accounted for by a spin coupling mechanism. Indeed, the nearest excited state is the ^{1}A(1) state. The small energy separation between the triplet and the ^{1}A(1) state (1.3 and

3.1 kcal mol^{-1} for [**1**·O_2] and [**2**·O_2], respectively) can therefore make spin-orbit coupling a reasonable mechanism that allows the reaction to proceed onto a singlet potential energy surface (see Figures 9 and Figure 10).

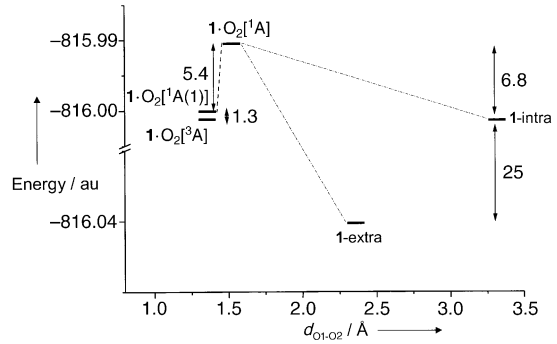

Figure 9. Diagram of energy minima (au) for the reaction **1** + O_2. Energy differences are shown in kcal mol^{-1}.

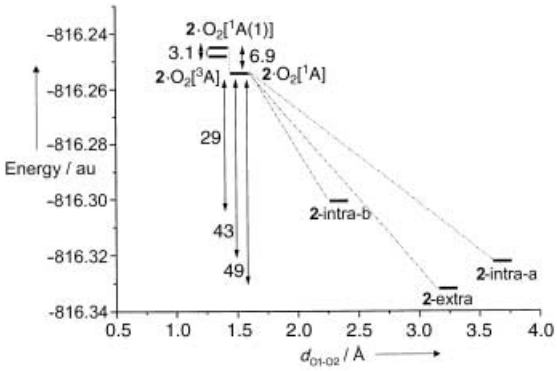

Figure 10. Diagram of energy minima (au) for the reaction **2** + O_2. Energy differences are shown in kcal mol^{-1}.

The close resemblance of the geometries of the molecules in the ^{3}A (Figure 4a and b) and in the ^{1}A(1) (Figure 6a and b) states supports this view. For the next step of the reaction, that is, the formation of the peroxy intermediate in the ^{1}A state, we see that this species lies at higher energy in [**1**·O_2] (5.4 kcal mol^{-1} from the ^{1}A(1) state), while it is stabilized by 6.9 kcal mol^{-1} in [**2**·O_2]. In both cases, however, the energy differences are still in the order of vibrational energies and the peroxy intermediates can be reached through an avoided crossing between the two singlet states. The energy required by [**1**·O_2] to reach the ^{1}A can easily come from the enthalpy gain of the first step. The protonation of the substrate seems to affect the energetics of the two pathways, confirming the importance of the asymmetry/protonation of the bound substrates as one of critical features claimed to be able to give different catalyzed products.[8, 17]

The presence of a proton and, therefore, of the asymmetry in the Ir–O bonds induces significant structural differences among two closely related systems, even in the first steps of the reactions, and can justify possible differences in their reactivity.

In a further step of calculations, aimed to rationalize the evolution from this peroxide intermediate to the final open chain products, the ^{1}A surfaces for [**1**·O_2] and [**2**·O_2] were scanned in order to locate the minima for the extra- and intradiol derivatives. The surfaces were scanned by performing independent geometry optimizations starting from the computed intermediates and varying the position of dioxygen, in particular increasing the O1-O2 bond length. Several structures that correspond to relative minima on the potential surface were met. They are depicted in Figures 11 and 12 for [**1**·O_2] and [**2**·O_2], respectively, together

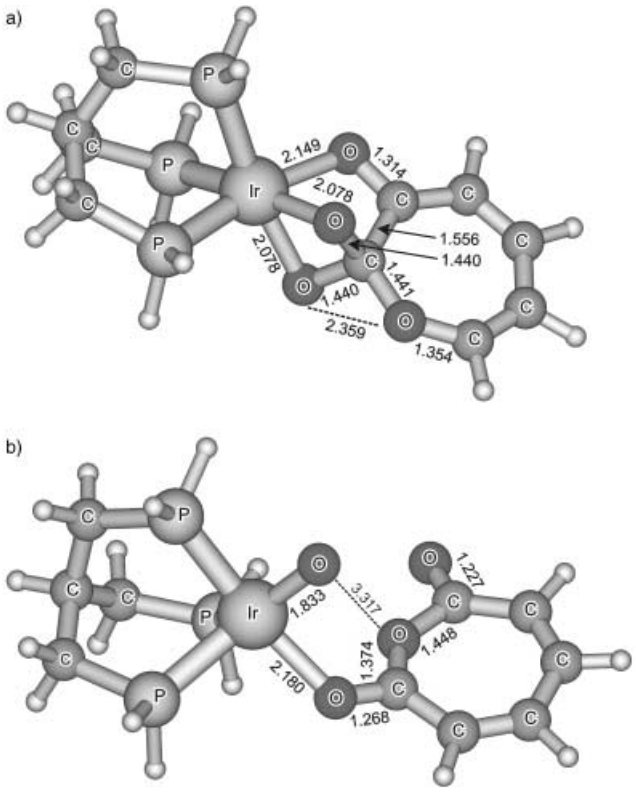

Figure 11. Optimized structures: a) **1**-extra; b) **1**-intra. Relevant bond distances (Å) are shown.

with the most relevant geometrical parameters. For [(triphosH)Ir^{III}(CT)(O_2)]$^+$ two distinct minima were computed corresponding to intra- and extradiol cleavage; these are shown in Figure 11a and b, and can be labeled **1**-extra and **1**-intra, respectively. For [(triphosH)Ir^{III}(CTH)(O_2)]$^{2+}$ three minima were computed one for the extradiol cleavage, labeled **2**-extra (Figure 12), and the other two for the intradiol cleavage reaction, **2**-intra-a and **2**-intra-b (Figure 12b and c).

The **1**-intra (Figure 11b) and the **2**-intra-a (Figure 12b) intermediates have similar structures with the iridium atom five-coordinate in a distorted trigonal-bipyramidal environment. The CT and CTH ligands were transformed in ε-keto-lactone species, which coordinate the iridium center with one oxygen. A further three positions in the coordination sphere are occupied by the P atoms of the triphosH ligand, and the fifth coordination site is filled by an oxygen atom, in **1**-intra, and by an hydroxyl group in **2**-intra-a. The formation of the oxide in **1**-intra makes the Ir–O(ε-keto-lactone) distance longer than that found in **2**-intra-a (1.180 vs. 2.125 Å).

The geometry of the **2**-intra-b intermediate (Figure 9c) differs from the previous ones. The iridium is still five-

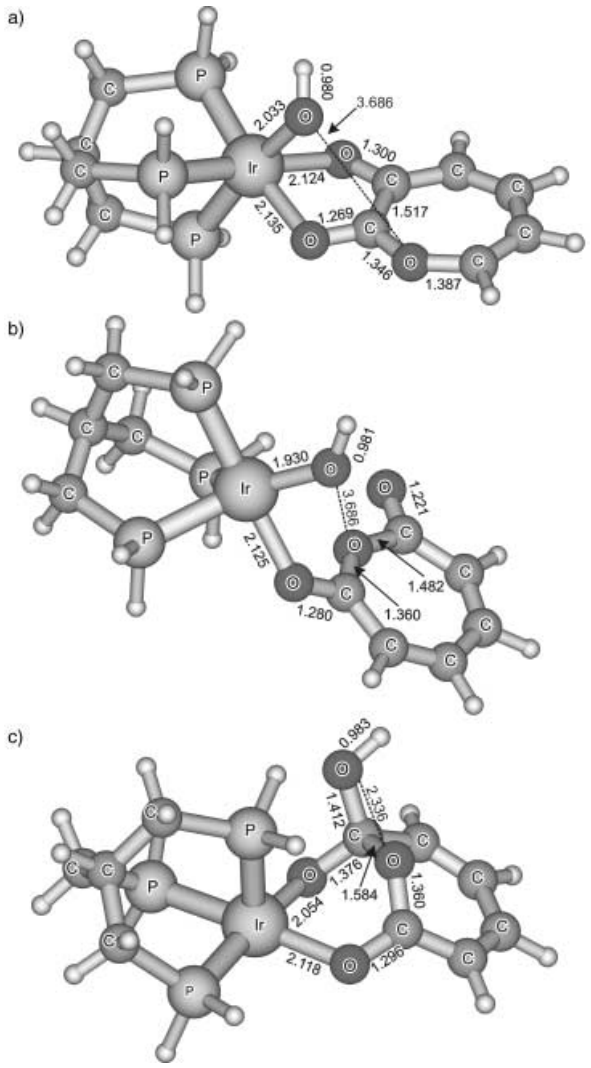

Figure 12. Optimized structures: a) **2**-extra; b) **2**-intra-a; c) **2**-intra-b. Relevant bond distances (Å) are shown.

coordinate, but in a distorted square pyramidal environment with the a ε-hydroxy-keto-lactone acting as bidentate ligand in the equatorial plane. All our attempts to locate a similar minimum on the ^{1}A potential surface for [**1**·O_2] failed. This could be due to the absence of the stabilization of the large negative charge of the ring, which in [**2**·O_2] is partially stabilized by the proton. Solvent effects may be relevant to the stabilization of this intermediate, but were not included in the calculations.

The geometry of the intermediates of the extradiol cleavage reactions also depends on the presence of the proton. Both in **1**-extra (Figure 11a) and **2**-extra (Figure 12a) the iridium atom is six-coordinate, but in **2**-extra, a hydroxyl group binds in the axial position of a distorted octahedron completing the coordination of Ir, while the axial oxygen in **1**-extra moves directly to attack the α-keto-lactone ring to giving the species shown in Figure 11a. In **2**-extra a α-keto-lactone is formed that acts as a bidentate ligand towards the iridium atom. It is worthwhile to note that Lin et al.[10t] suggested that the pyridinium salt in the TACN/$FeCl_2$/CTH system was claimed to act as proton donor to assist the cleavage of the O1–O2 bond in the Criegee[4] rearrangement. The migration of the proton from the catechol oxygen atom to that bound to the iridium atom seems to be in agreement with the mechanism claimed in reference [10t] (see below).

The total energies computed for all of the above mentioned species are shown in Figures 9 and 10 for [**1**·O_2] and [**2**·O_2], respectively. On the abscissa we report the computed O1–O2 distances, which allow us to discriminate between the minima like an intrinsic reaction coordinate. As expected, ^{3}A and ^{1}A(1) states are quite close in energy both in [**1**·O_2] and [**2**·O_2], and, therefore, can be admixed by spin-orbit coupling. The energies of formation of the intermediates computed for the ^{1}A state differ in [**1**·O_2] and [**2**·O_2], while in [**2**·O_2], the formation of the ^{1}A intermediate is exothermic by $\sim$ 6 kcal mol^{-1}, in [**1**·O_2] the same intermediate is higher in energy ($\sim$ 7 kcal mol^{-1}) than the ^{3}A state. Both in [**1**·O_2] and in [**2**·O_2] the intermediates leading to extradiol cleavage are more stable than those corresponding to the intradiol reaction (25 kcal mol^{-1} for [**1**·O_2] and 6 kcal mol^{-1} for [**2**·O_2]).

From the above calculations it is apparent that from [(triphosH)Ir^{III}(CTH)(O_2)]$^{2+}$ both intra- and extradiol cleavage can be obtained, while in [(triphosH)Ir^{III}(CT)(O_2)]$^+$ the extradiol reaction is expected to be more exothermic and favored, if enthalpy governs the reaction.

Looking now to the specific reaction occurring between [(triphos)M(dtbc)]$^+$ (M = Rh, Ir) and O_2, experimental findings showed that the adducts [(triphos)M(dtbc)O_2]$^+$ can evolve to oxygenated compounds giving extra- and intradiol products, if an excess of $DBTCH_2$ is added to the solution.[10r] Under these conditions it is reasonable to think that DBTC undergoes protonation originating the DBTCH complex and, on the basis of our calculation, a mixture of both intra- and extradiol products are expected. As a matter of fact, it was experimentally found[10r] that with Rh both extra- and intradiol derivatives are formed at low temperature (at $-15\,^\circ$C the ratio extra/intra was 1:2). In turn, the Ir complex, reacts with O_2 at 30 °C and high pressure, providing again both extra- and intradiol products; however in the opposite ratio of 13:1.

Considering the formal electronic similarity existing between Fe^{II} and Rh^{III}/Ir^{III}, a theory can be made to correlate our theoretical predictions with the experimental results by Lin et al.[10t] on the TACN/$FeCl_2$/CT and the TACN/$FeCl_2$/CTH systems. TACN/$FeCl_2$/CT system always selectively gives the extradiol product that we computed as 25 kcal mol^{-1} more stable than the intradiol product (see Figure 9). In the presence of pyridinium hydrochloride, the TACN/$FeCl_2$/CTH system gives a mixture of 4:1 extra/intra products, in agreement with what has been already discussed for that of Rh– and Ir–CTH derivatives. The energy scheme of Figure 10 doesn't exclude the possibility of the formation of a mixture of products, whose relative amounts could be dependent on different kinetics of the reactions and on the actual environment.

Indeed the fact that in the *absence* of the pyridinium salt the TACN/$FeCl_2$/CTH system gives an extra/intra ratio of 1:15, suggests that kinetic factors depending, for example, on proton availability/mobility can alter the intra/extra ratio. The present calculations seem, therefore, to be able to qualitatively reproduce not only the experimental findings reported for the dioxygenation reaction catalyzed by the iridium

complex, but also those reported for the isoelectronic Fe^{II} complexes under a variety of experimental conditions.

As a final point a comparison with reactions catalyzed by the iron(II) dioxygenases can be also attempted. We know that these enzymes, which give extra-diol products, bind catechols as monoanions and, therefore, they can be assimilated to TACN/$FeCl_2$/CTH in the *presence* of pyridinium hydrochloride. The much higher selectivity observed in the enzymes could be explained on the basis of an assisted proton transfer from a specific spatial arrangement of residues present in the active site. As a matter of fact, Tyr250 was claimed to act as a proton shuttle between the catecholic substrate and His241.[8]

Conclusion

On the basis of the experimental data available for Ir and Rh catecholate complexes, the reported DFT/B3LYP computational approach gave an important insight into the understanding of their reactivity in the presence of dioxygen. The first steps taking place in the reaction were computed suggesting the spin-orbit coupling as the most likely mechanism supposed for the reaction that leads to the formation of the diamagnetic iridium peroxy-bridged adduct. Indeed the formation of a stable oxygen adduct in which the oxygen molecule bridges both the metal center and one carbon atom of the catechol moiety is computed in agreement with the experimental findings. The calculated structural features of the adduct agree quite reasonably with the experimental structure.

A stable peroxy-bridged complex was also computed with the protonated monodentate catechol, but the structural parameters somehow differ from the structure in which the catechol binds as a bidentate ligand. Both peroxy-bridged complexes were shown to be able to give thermodynamically favored products; the introduced differences in the metal–catechol distances by the presence of a single proton are then suggested to give the potential difference in activation in the catechol itself.

The computational results also seem to be in good qualitative agreement with the reactivity of the TACN/$FeCl_2$/DBTC and TACN/$FeCl_2$/DBTCH systems. This supports the new hypothesis of a common intermediate for the extra- and intradiol cleavage reactions. The claimed importance of the proton availability as the critical factor to favor specific extra or intra products has been also supported.

An extension to the extradiol dioxygenase enzymatic reactions can be also successfully made, so that we feel confident that the main conclusions obtained here are transferable to the catalytic centers of iron(II) dioxygenases, giving a breakthrough on the general strategy of natural enzymatic systems.

Acknowledgements

This work was perfomed in the framework of NOHEMIP Network and supported by EC contracts FMRX-CT980174 and ICA2-CT-2000-10006. The financial support of Progetto Finalizzato Biotecnologie e Progetto Rischi Industriali of CNR together with COFIN2000 is gratefully acknowledged.

[1] "Perspective in Bioremediation. Technologies for Environmental Improvement"F. Briganti, I. M. C. M. M. Rietjens, A. Scozzafava, B. Tyrakowska, C. Veeger, *NATO ASI Ser. 3* **1997** *19*, 25.

[2] a) P. J. Chapman, in *Degradation of Synthetic Organic Molecules in the Biosphere*, National Academy of Sciences, Washingon, D.C, **1972**, p. 17; b) R. C. Bayly, and M. G. Barbour, *Microbial Degradation of Aromatic Compounds* (Ed.: D. T. Gibson), Marcel Dekker, New York, **1984**, p. 274; c) D. T. Gibson, V. Subramanian, in *Microbial Degradation of organic Molecules* (Ed.: D. T. Gibson), Marcel Dekker, New York, **1984**, p. 181; d) S. Dagley, *Dev. Ind. Microbiol. Ser.* **1984**, *25*, 53.

[3] *Microbial Degradation of Organic Molecules* (Ed.: D. T. Gibson) Marcel Dekker, New York, **1984**.

[4] L. Que Jr., R. Y. N. Ho, *Chem. Rev.* **1996**, *96*, 2607.

[5] a) D. H. Ohlendorf, J. D. Lipscomb, P. C. Weber, *Nature* **1998**, *336*, 403; b) D. H. Ohlendorf, A. M. Orville, J. D. Lipscomb, *J. Mol. Biol.* **1994**, *244*, 586; c) M. W. Vetting, C. A. Earhart, D. H. Ohlendorf, *J. Mol. Biol.* **1994**, *236*, 372; d) M. W. Vetting, D. H. Ohlendorf, *Structure* **2000**, *8*, 429.

[6] a) S. Han, L. D. Eltis, K. N. Timmis, S. W. Muchmore, J. T. Bolin, *Science* **1995**, *270*, 976; b) A. Kita, S. I. Kita, I. Fujisawa, K. Inaka, T. Ishida, K. Horiike, M. Nozaki, K. Miki, *Structure* **1998**, *7*, 25; c) K. Sugimoto, T. Senda, H. Aoshima, E. Masai, M. Fukuda, Y. Mitsui, *Structure* **1999**, *7*, 953; d) G. P. Titus, H. A. Mueller, J. Burgner, S. de Cordoba Rodriguez, M. A. Penalva, D. E. Timm, *Nat. Struct. Biol.* **2000**, *7*, 542.

[7] T. D. H. Bugg, C. J. Winfield, *Nat. Prod. Rep.* **1998**, *15*, 513

[8] F. H. Vaillancourt, C. J. Barbosa, T. G. Spiro, J. T. Bolin, M. W. Blades, R. F. B. Turner, L. D. Eltis, *J. Am. Chem. Soc.* **2002**, *124*, 2485.

[9] a) A. M. Orville, J. D. Lipscomb, D. H. Ohlendorf, *Biochemistry* **1997**, *36*, 10052; b) M. W. Vetting, D. A. D'Argenio, L. N. Ornston, D. H. Olhendorf, *Biochemistry* **2000**, *39*, 7943; c) T. E. Elgren, A. M. Orville, K. A. Kelly, J. D. Lipscomb, D. H. Olhendorf, L. Que, Jr., *Biochemistry* **1997**, *36*, 11504; d) C. A. Tyson, *J. Biol. Chem.* **1975**, *250*, 1765; e) L. Que Jr., R. M. Epstein, *Biochemistry* **1981**, *20*, 2545.

[10] a) L. Que, Jr., R. C. Kolanzczyk, L. S. White, *J. Am. Chem. Soc.* **1987**, *109*, 5373; b) H. G. Jang, D. D. Cox, L. Que Jr., *J. Am. Chem. Soc.* **1991**, *113*, 9200; c) S. Fuji, M. Duda, M. Pascaly, B. Krebs, *Chem. Commun.* **1997**, 835; d) R. Viswananthan, M. Palaniandavar, T. Balasubramarian, T. D. Muthiah, *Inorg. Chem.* **1998**, *37*, 2943; e) T. Funabiki, T. Yamazaki, A. Fukui, T. Tanaka, S. Yashida, *Angew. Chem.* **1998**, *110*, 527; *Angew. Chem. Int. Ed.* **1998**, *37*, 513; f) W. O. Koch, H.-J. Krüger, *Angew. Chem.* **1995**, *107*, 2928; *Angew. Chem. Int. Ed. Engl.* **1995**, *34*, 2671; g) P. Mialane, L. Tchertanov, F. Banse, J. Sainton, J.-J. Girerd, *Inorg. Chem.* **2000**, *39*, 2440; h) T. Funabiki, A. Mizoguchi, T. Sugimoto, S. Tada, M. Tsugi, H. Sakamoto, S. Yoshida, *J. Am. Chem. Soc.* **1986**, *108*, 2921; i) A. Dei, D. Gatteschi, L. Pardi, *Inorg. Chem.* **1993**, *32*, 1389; l) M. Ito, L. Que, Jr., *Angew. Chem.* **1997**, *109*, 1401; *Angew. Chem. Int. Ed. Engl.* **1997**, *36*, 1342; m) G. Lin, G. Reid, T. D. H. Bugg, *Chem. Commun.* **2000**, 1119; n) E. L. Spence, G. J. Langley, T. D. H. Bugg, *J. Am. Chem. Soc.* **1996**, *118*, 8336; o) J. Sanvoisin, G. J. Langley, T. D. H. Bugg, *J. Am. Chem. Soc.* **1995**, *117*, 7836; p) R. Muller, F. Z. Lingsens, *Z. Naturforsch. Teil C* **1989**, *44*, 207; q) C. Bianchini, F. Frediani, F. Laschi, A. Meli, F. Vizza, P. Zanello, *Inorg. Chem.* **1990**, *29*, 3402; r) P. Barbaro, C. Bianchini, C. Mealli, A. Meli, *J. Am. Chem. Soc.* **1991**, *113*, 3183; s) P. Barbaro, C. Bianchini, P. Frediani, A. Meli, F. Vizza, *Inorg. Chem.* **1992**, *31*, 1523; t) G. Lin, G. Reid, T. D. H. Bugg, *J. Am. Chem. Soc.* **2001**, *123*, 5030; u) P. Barbaro, C. Bianchini, K. Linn, C. Mealli, A. Meli, F. Vizza, F. Laschi, P. Zanello, *Inorg. Chim. Acta* **1992**, *198–200*, 31

[11] a) M. H. Gubelmann, A. F. Williams, *Struct. Bonding* **1983**, *55*, 1; b) H. Mimoun, *Comprehensive Coordination Chemistry, Vol. 6*, (Ed.: G. Wilkinson) Pergamon, Oxford, **1987**, 318.

[12] T. Funabiki, T. Yamazaki, *J. Mol. Catal A* **1999**, *150*, 37.

[13] A. Bassan, M. R. A. Blomberg, P. E. M. Siegbahn, L. Que, Jr., *J. Am. Chem. Soc.* **2002**, *124*, 11056.

[14] "Oxygenases and Model Systems" T. Funabiki, in *Catalysis by Metal Complexes Vol 19* (Eds.: R. Ugo, B. R. James), Kluwer Academic, Dordrecht, **1997**, p. 1.

[15] a) M. Fujiwara, L. A. Golovleva, Y. Saeki, M. Nozaki, O. Hayaishi, *J. Biol. Chem.* **1975**, *250*, 4848; b) S. Murakami, T. Okuno, E. Matsu-

mura, S. Takenaka, R. Shinke, K. Aoki, *Biosci. Biotechnol. Biochem.* **1999**, *63*, 859.
[16] A. Bencini, E. Bill, F. Mariotti, F. Totti, A. Scozzafava, A. Vargas, *Inorg. Chem*. **2000**, *39*, 1418.
[17] L. Shu, Y-M. Chiou, A. M. Orville, M. A. Miller, J. D. Lipscomb, L. Que, Jr., *Biochemistry* **1995**, *34*, 6649.
[18] A. D. Becke, *J. Chem. Phys.* **1993**, *98*, 5648.
[19] a) P. J. Hay, W. R. Wadt, *J. Chem. Phys.* **1985**, *82*, 270; b) W. R. Wadt, P. J. Hay, *J. Chem. Phys.* **1985**, *82*, 284; c) P. J. Hay, W. R. Wadt, *J. Chem. Phys.* **1985**, *82*, 299.
[20] a) L. Vaska, *Science* **1963**, *140*, 809; b) L. Vaska, *Acc. Chem. Res.* **1976**, *9*,175; c) R. S. Drago, T. Beugelsdijk, J. A. Breese, J. P. Cannady, *J. Am. Chem. Soc.* **1978**, *100*, 5374.
[21] The energy calculation of ^{1}A and ^{3}A was performed by using a single Slater determinant corresponding to the configurations (xz^{*2}) and ($xz^{*1}\,\pi^{*1}$). The energy of ^{1}A(1) was computed following the procedure outlined by Zigler et al; see: T. Ziegler, E. J. Baerends, P. Vernooijs, *Theor. Chim. Acta* **1977**, *43*, 261 from the SCF energy of the determinant ($xz^{*1}\,\pi^{*1}$) with $M_s = 0$ and of ^{3}A. The calculations of ^{3}A and ^{1}A(1) were spin unrestricted
[22] a) S. P. McGlynn, T. Azumi, M. Kinoshita, *Molecular Spectroscopy of the Triplet State*, Prentice-Hall, Englewood Cliffs, **1969**; b) L. Salem, C. Rowland, *Angew. Chem.* **1972**, *84*, 86; *Angew. Chem. Int. Ed. Engl.* **1972**, *11*, 92; c) S. Shaik, N. D. Epiotis, *J. Am. Chem. Soc.* **1978**, *100*, 18; d) N. D. Epiotis, *Theory of Organic Reactions*, Springer, Berlin, Heidelberg **1978**.
[23] *Handbook of Chemistry and Physics* (Eds.: R. C. Weast, M. J. Astle, W. H. Beyer) 67th edition, CRC Boca Raton, Florida **1986–7**.

Received: December 30, 2003 [F4710]

